The International Journal of Engineering and Science (IJES)
|| Volume || 15 || Issue 11 || November || Pages || PP 11-26 || 2026 ||
ISSN (e): 2319-1813 ISSN (p): 2319 – 1805

A Box–Jenkins-Based Feedforward Control Approach for Industrial Power Factor Management Using Multiple Electrical Measurements

[1]Kean Eng NG, *ICA40 Sdn Bhd, A1, Jalan BA/3, Kawasan Perusahaan Bukit, Malaysia*
[2]Chee Kit Ho, *ICA40 Sdn Bhd, A1, Jalan BA/3, Kawasan Perusahaan Bukit, Malaysia*
[3]Kean Thong NG, *ICA40 Sdn Bhd, A1, Jalan BA/3, Kawasan Perusahaan Bukit, Malaysia*
[4]Yuichi ANADA, *Hokkaido Information University, Hokkaido, Japan*
[5]Takanori YAMAKITA, *Hokkaido Information University, Hokkaido, Japan*
[6]Tsukasa HOKIMOTO, *Hokkaido Information University, Japan*
Corresponding Author : hock@ica40.com

----------ABSTRACT----------
Power factor (PF) fluctuations in industrial equipment can affect power-system performance and create exposure to tariff surcharges. This study applies Box–Jenkins transfer-function modelling to multiple electrical measurements obtained from a robotic welding machine in a Malaysian factory. Measured industrial time-series data were used in numerical control experiments and simulation; calculated current-control commands were not physically implemented on the machine. Individual factor-specific PF predictions were combined using two weighting schemes: minimisation of historical fitting errors (Method A) and minimisation of one-step-ahead prediction errors (Method B). In the reported rolling-window comparisons, Method B produced fewer adverse negative deviations than Method A across all examined thresholds for multivariable feedforward control. Adding ARMA-based feedback did not further reduce those downside frequencies in the reported comparisons. The findings show the value of prediction-oriented weighting in a Box–Jenkins-based numerical control evaluation under the investigated operating conditions.

Keywords: feedforward control, electric power, transfer function model, statistical control, prediction

---

Date of Submission: 01-11-2026 Date of acceptance: 10-11-2026

I. INTRODUCTION

Manufacturing facilities increasingly rely on automated production equipment and digital monitoring systems, yet smaller enterprises often face constraints in the expertise, investment and operational resources required to translate measured data into useful decisions. In Malaysia, the National Policy on Industry 4.0 (Industry4WRD) provides a framework for industrial upgrading and digital adoption [1][2]. Nevertheless, implementation challenges remain, particularly in the integration of Internet of Things (IoT), cyber-physical systems and data analytics into existing production environments [3]. Intelligent monitoring and condition-based maintenance offer opportunities to improve machine availability and reduce unplanned interruptions [4], while longstanding issues in equipment condition and workplace practices can continue to affect operational performance [5].

Industrial electricity costs may depend on maximum demand and power factor (PF), which are distinct billing and engineering quantities. Demand management addresses load peaks [6], whereas PF relates active to apparent power. Capacitor banks are conventional compensation devices [7][8]. This study examines a complementary, data-driven approach to anticipating PF disturbances; it does not claim to replace reactive-power compensation.

Power-system control has been examined through physics-based approaches, including phase adjustment and compensation techniques [9][10], and through model-based state estimation such as Kalman filtering [11]. Related

applications demonstrate the broader potential of statistical estimation in dynamic systems [12][13][14][15]. These approaches provide useful foundations, but an industrial practitioner also needs a method that can be developed from historical operating data and updated as equipment conditions change.

This study therefore explores a Box–Jenkins transfer-function approach [16] for predicting the dynamic relationship between PF and measured electrical variables. The central proposition is operational: identify measurable fluctuations, estimate their delayed effects on PF, and calculate a feedforward control response; where residual disturbances are predictable, supplement this response using feedback. The initial framework distinguishes monitored voltage from a proposed current-related control input, before the subsequent sections of the full paper extend the observation system to multiple physical factors.

The objectives are to:

(i) characterise PF fluctuations from operating robotic-welding equipment;

(ii) identify dynamic relationships between monitored electrical factors and PF;

(iii) calculate and evaluate current adjustments using Box–Jenkins feedforward control in numerical experiments; and

(iv) compare alternative multivariable weighting and combined feedforward–feedback strategies.

The study uses industrial measurements as the basis for numerical control experiments and simulation. Rolling-window forecasts and calculated control responses are model-based outcomes, not measured closed-loop control results.

II. POWER MONITORING AND PROBLEM DEFINITION

Industrial equipment and measurement architecture

The case study uses a Panasonic TM-1400GIII robotic welding machine operating in a Malaysian factory. Figure 1 presents the measurement arrangement. An electronic multi-measuring instrument (Mitsubishi ME96SSRB-MB) is installed at the switchboard to acquire the machine's electrical operating information. Current is measured through a current transformer and voltage is measured from the supply. Signals are digitised by the measuring instrument and transferred to an industrial computer (Dell Embedded Box PC 5000) through MODBUS RTU over an RS485 interface. Recorded variables include PF, voltage, current, active power and reactive power.

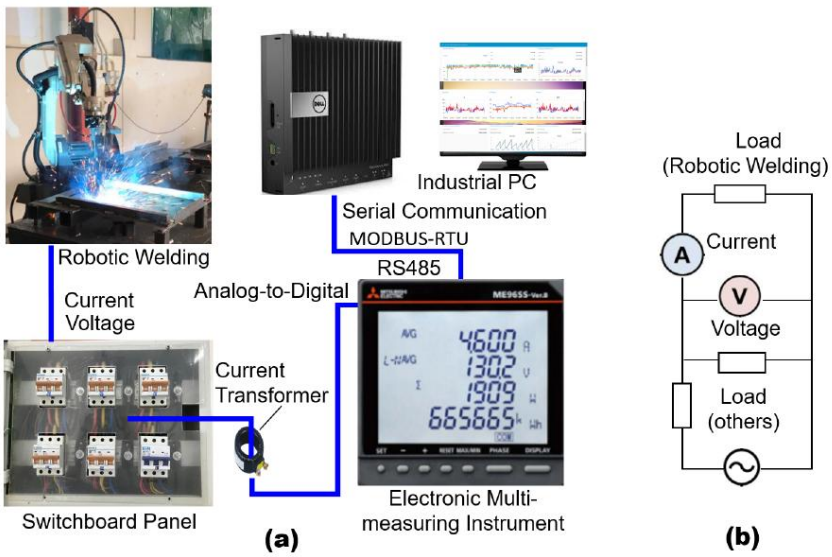


Figure 1: Measurement system and current/voltage measurement circuit.

The instrumentation software retrieves readings at one-second intervals. For time-series analysis, observations were sampled at 12-second intervals. Figure 2 presents the record from 17 May 2021, approximately 08:31–17:37,

containing 2,634 time points. The welding machine operated during the earlier part of the record, with further changes in operating condition later in the day.

Observed fluctuations in power factor

Figure 2 plots PF, voltage, current, active power and reactive power against the same time index. PF varies substantially during operation, including periods below the threshold discussed in the introduction. Variations in current and voltage occur over related periods, while active and reactive power also change with machine operation. These co-movements motivate an investigation of dynamic relationships; they do not by themselves establish that variation in voltage or current independently causes the observed PF change.

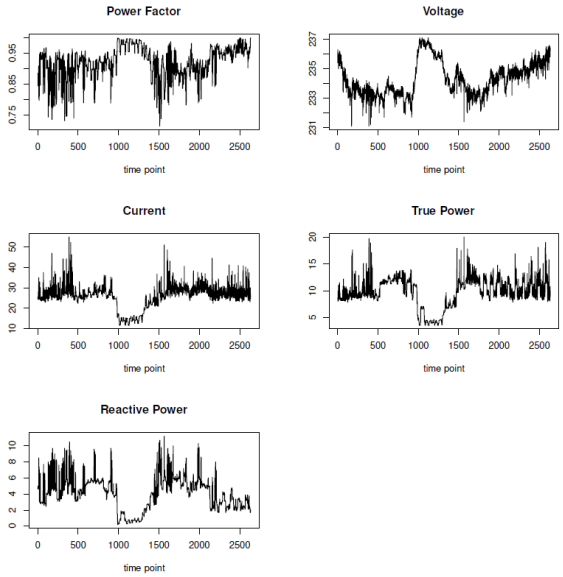


Figure 2: Observed time series of PF, voltage, current, active power and reactive power.

For interpretation, the power factor at time t is related to active power P_t and reactive power Q_t by:

$PF_t = P_t / \sqrt{(P_t^2 + Q_t^2)}$ [descriptive PF relationship]

This relationship helps interpret the observed variation in PF as active and reactive power change, without by itself establishing a controllable relationship between current and PF.

From monitoring to a control problem

Monitoring alone can identify low-PF episodes but cannot specify an intervention. A control method must determine :-

(i) which measured signal is informative before a PF change occurs,
(ii) the delay between that signal and its effect on PF,
(iii) the response of PF to a feasible control adjustment and
(iv) whether the calculated command can be applied through a feasible welding-machine control interface.

These are time-dependent questions suited to Box–Jenkins transfer-function identification [16].

The desired outcome is to reduce undesirable PF fluctuations, especially negative excursions, while maintaining the operational requirements of the welding process. Two outcomes should be assessed separately: reduction of PF variation and tracking of a specified PF target. The former does not automatically ensure the latter. Similarly, the current measured by the electrical meter is not necessarily a controllable setpoint; a practical control system must identify the equipment interface that can make any proposed adjustment.

III. PROPOSED BOX-JENKINS CONTROL METHODOLOGY

Control concept and variable definitions

The proposed strategy follows a two-layer structure: feedforward action based on a monitored disturbance, and feedback action based on the remaining predictable error. Let Y_t denote measured PF, Z_t denote monitored voltage and X_t denote measured current at discrete time t. For model estimation, deviations from historical means are distinguished from deviation from the required PF target T. In particular, the target-tracking error is $Y_t - T$; a mean-centred response is not interchangeable with this target-tracking error.

The transfer-function formulation uses the mean-centred PF response $\tilde{Y}_t = Y_t - \bar{Y}$, where $\bar{Y}$ is the historical mean PF over the estimation period. Performance against the specified PF target T is evaluated separately using $\tilde{Y}_t^* = \log(Y_t) - \log(T)$, with T = 0.90. The target-relative logarithmic deviation is not additionally mean-centred.

In the first-stage model, voltage is the monitored disturbance input. Measured current is distinguished from the current-control command calculated by the Box–Jenkins controller. The calculated commands were evaluated in numerical experiments and simulation; no physical current adjustment by the controller is reported. The Box–Jenkins method represents lagged effects rather than assuming instantaneous response.

The central modelling assumption is an additive dynamic response, expressed compactly as:

$$\tilde{Y}_t = GZ(B)Z_{t-\beta} + GX(B)X_{t-(f+1)} + N_t \quad \text{[Equation (4)]}$$

The additive decomposition is a modelling assumption and requires the voltage and current effects to be identified while accounting for their mutual dependence. The transfer-function specification and assumptions are detailed in Appendix A.

All symbols and notation follow the nomenclature in Appendix B.3.

Feedforward compensation of an observed disturbance

Feedforward control acts before the resulting PF deviation is fully realised. After estimating the voltage-to-PF and current-to-PF dynamic relationships, the method calculates a current-related command intended to offset the predictable voltage contribution. The required response depends on both the magnitude and the relative timing of these relationships. If voltage changes become observable sufficiently early, the controller may use the measured input. If the current-control response is slower, a forecast of future voltage is required.

Cancelling the modelled voltage contribution gives the theoretical feedforward current-control level:

$$X_tFF = -GX^{-1}(B)GZ(B)Z_{t-(b-f-1)} \quad \text{[Equation (5)]}$$

Here GZ(B) and GX(B) are the monitored-voltage and current-response transfer functions, respectively; b and f+1 denote their response delays. The feedforward control law is derived as Equation (5) in Appendix A. Calculated commands are model-based; Equation (A1) distinguishes incremental from absolute command representations.

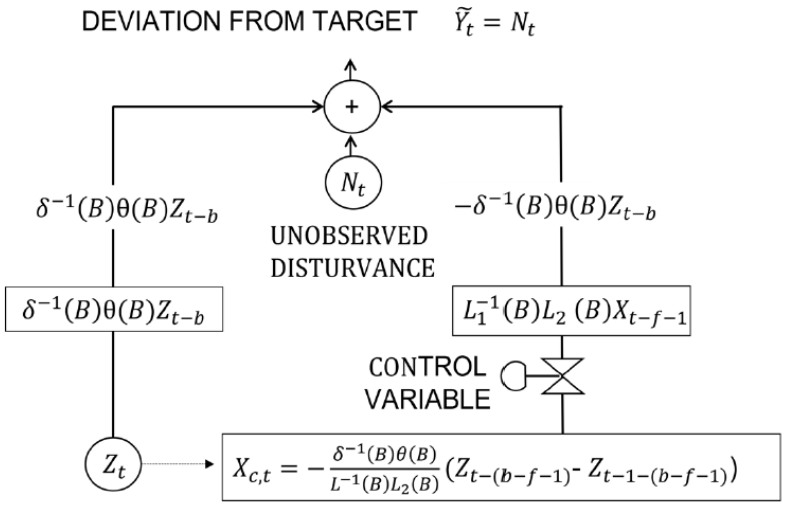


Figure 3: Feedforward control scheme.

Figure 3 presents the theoretical feedforward cancellation scheme. Its "deviation from target" label is a control-design interpretation; the transfer-function derivation uses the mean-centred response $\tilde{Y}_t$. The ideal linear cancellation leaves the residual disturbance, but physical performance may differ because of identification error, timing and actuator limits. No measured post-actuation PF results are claimed.

Feedback compensation of predictable residual disturbances

Feedforward control cannot remove disturbances that are not explained by the monitored voltage signal. Some of those residual fluctuations may nevertheless contain temporal patterns. The Box–Jenkins approach examines whether an autoregressive moving-average (ARMA) model can describe the disturbance sequence and forecast its future value. A feedback correction is then calculated for the time at which the control action is expected to influence PF.

To forecast the remaining disturbance N_t, the Box–Jenkins approach represents its temporal dependence with an ARMA model:

$$\varphi(B)N_t = \omega(B)a_t \quad \text{[Equation (7)]}$$

Where a feasible feedback correction X_t^{fb} can be calculated from the forecast disturbance, the conceptual combined control level is:

$$X_t\text{total} = X_tFF + X_tFB \quad \text{[Equation (A3)]}$$

The disturbance forecast is obtained from historical residuals and projected to the time at which the current action takes effect. Feedforward compensates the predicted voltage contribution, while feedback targets predictable residual error. Appendix A gives the forecast and feedback-control derivations, including the necessary assumptions about delay, inverse filters and residual estimation.

The two control contributions may be combined only when they are defined against the same reference and the underlying additive model is valid. Residuals must also be calculated consistently: when current control is active, the modelled current-control contribution must be subtracted alongside the voltage contribution. A voltage-only residual can be interpreted as the unexplained disturbance only under an explicit zero-control or baseline condition.

Experimental implementation and evaluation procedure

Electrical measurements were obtained from the operating robotic welding machine using the instrumentation described in Section II. The recorded time series were used to estimate response delays and identify Box–Jenkins transfer functions. Feedforward and combined feedforward–feedback current-control commands were calculated and assessed through numerical experiments and simulation; the calculated commands were not physically applied to the welding machine. The evaluation compares model-based control responses across the specified observation systems.

The numerical evaluation uses rolling-window model fitting and forecasting to compare observation-variable selections and feedforward versus combined feedforward–feedback methods. Reported forecast errors and calculated control trajectories are model-based results, not measurements of changes caused by physical current commands. PF variation and achievement of the PF = 0.90 target are assessed as distinct questions. The statistical control approach does not, by itself, establish that reactive-power compensation equipment can be removed.

The methodological contribution of this section is therefore the use of Box–Jenkins identification and disturbance prediction to inform a practical PF-control decision. The detailed mathematics supports this decision-making framework without constituting the principal focus of the paper.

IV. EXTENDING BOX-JENKINS MODELLING TO MULTIPLE OBSERVED FACTORS

The single-disturbance model in Section III uses voltage as the monitored input and current as the proposed manipulated variable. In a production environment, however, PF fluctuations can coincide with changes in several electrical measurements. The contribution of Section IV is therefore not another control mechanism; it is a way to combine information from several monitored factors without relying on one predictor throughout the operating cycle.

Four factors are identified by the labels used in the weighting plot: total power, reactive power, voltage and electric power. The measured time-series plot separately labels true (active) power. These source labels are retained without assuming that total power and electric power constitute independently defined electrical quantities. Current remains the control-related variable, not a fifth weighted factor.

Combining factor-specific PF predictions

For each monitored factor j, an individual Box–Jenkins transfer function provides a lagged PF-related output. Following the multivariable formulation, these filtered outputs are weighted to construct a composite observation signal Z^*_t (Method A) or Z^{**}_t (Method B). The composite signal then enters the overall PF-response transfer function, with the current-control contribution modelled separately (Appendix B.1).

Composite observation: $Z^*_t = \Sigma_j\, w_j\, \delta_j^{-1}(B)\theta_j(B)B^{bj}Z_t^{(j)}, \quad w_j \geq 0, \quad \Sigma_j\, w_j = 1$ [Method A; Appendix B.1]

Each $Z_t^{(j)}$ is a monitored factor and $\delta_j^{-1}(B)\theta_j(B)B^{bj}$ its fitted lagged contribution. The weighted composite observation is processed through the additional overall observation-side transfer function in the multivariable response model. Appendix B.1 defines both weighting objectives and the associated response models.

Two alternative weighting strategies

Factor-specific transfer-function orders are selected using the Akaike Information Criterion (AIC) [17]. Two weighting objectives are then compared. Method A minimises historical squared fitting errors; Method B minimises one-step-ahead squared PF prediction errors, using forecasts of inputs when required. Historical fit and next-step prediction performance need not be identical [18].

Approach	Weight selection	Operational interpretation

Method A: fitting-error weighting	Minimise historical squared errors	Emphasises explanation of the observed PF history
Method B: prediction-error weighting	Minimise one-step-ahead forecast errors	Emphasises prediction under changing conditions

Both strategies construct a weighted composite observation input from factor-specific transfer-function outputs. Method A selects weights using historical fitting errors; Method B uses one-step-ahead prediction errors. The composite input enters the observation-side PF response transfer function, alongside the separately identified current-to-PF response (Appendix B.1).

V. EXPERIMENTAL RESULTS AND MODEL-BASED PERFORMANCE EVALUATION

The investigation used industrial electrical measurements as inputs to Box–Jenkins numerical control experiments and simulation. This section reports the observed PF behaviour, dynamic-model diagnostics and comparative calculated control-robustness results. The rolling-window statistics evaluate model-based PF deviations; they are not measurements of the effect of physically applied control commands.

Data, target and evaluation design

The experimental reference target was PF = 0.90. The target-relative logarithmic deviation is $\tilde{Y}_t^* = \log(Y_t) - \log(T)$, with T = 0.90; therefore $\tilde{Y}_t^* = 0$ corresponds to PF = 0.90. This measure is distinct from the mean-centred response $\tilde{Y}_t$ used in Equations (1)–(4).

The target-relative log deviation describes PF relative to 0.90 and underlies the displayed target comparison. It is distinct from the mean-centred response used to state the general transfer-function model. The mean-centred and logarithmic target-relative representations are not algebraically interchangeable; the applicable response scale must be specified for interpreting fitted transfer functions.

The measurement record from the robotic welding machine was analysed at 12-second intervals. Each model-estimation window contains 150 observations (30 minutes). Figure 4 shows the measured PF series and a selected interval expressed as logarithmic deviation from the 0.90 reference.

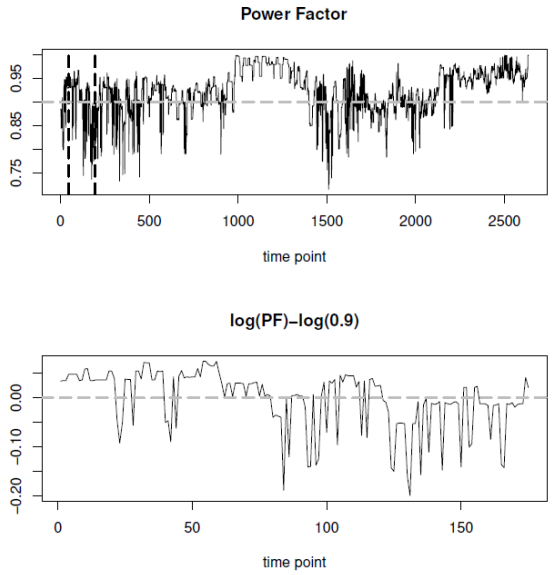


Figure 4: Measured records of power factor (upper: all operating hours, lower: 8:50 - 9:11)

The pronounced negative excursions in Figure 4 motivate evaluation of downside control robustness, rather than relying solely on average PF or overall variance.

For the comparative assessment, six observation systems were considered: multivariable Methods A and B and four single-factor baselines. Models were fitted on 150 observations, evaluated one step ahead, then advanced by five observations; this procedure generated 100 calculated control deviations. Separate illustrations consider responses up to 25 steps ahead. Appendix B retains the evaluation procedure and detailed results.

Evidence that the disturbance has forecastable structure

The electrical inputs exhibit different lagged associations with PF (Figure 5). These differences motivate the factor-specific dynamic relationships used in the Box–Jenkins approach.

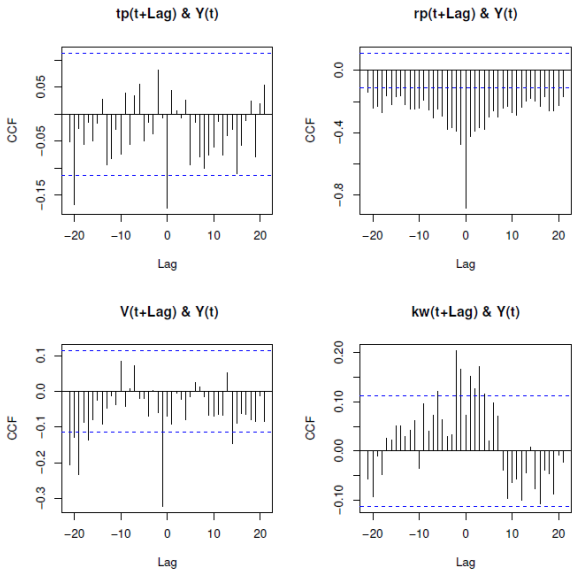


Figure 5: Cross-correlation between each monitored factor and PF (upper left: true power; upper right: reactive power; lower left: voltage; lower right: electric power).

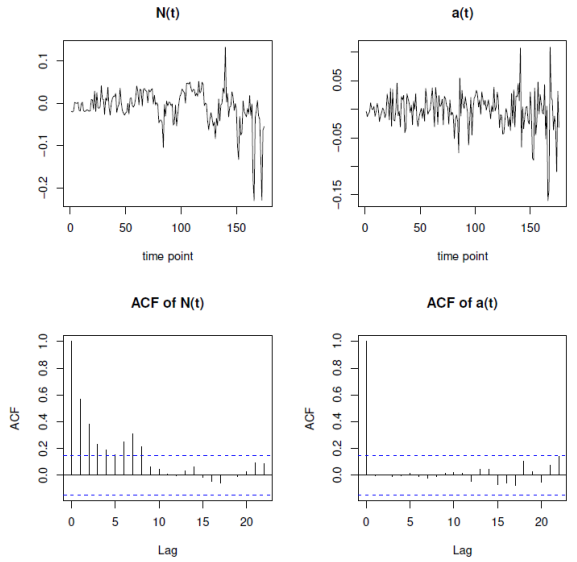


Figure 6 compares the estimated disturbance N_t and the ARMA innovation a_t. The fitted disturbance exhibits autocorrelation, whereas the innovation has substantially weaker residual autocorrelation. This supports using the ARMA model to represent the forecastable part of the remaining disturbance [19].

Figure 6: Time variation of disturbance residual N_t and innovation a_t (top) and their autocorrelation coefficients (bottom).

The reported disturbance variance Var (N) describes the residual variation of the combined response model; Var(a) describes innovation variance in Equation (7). The innovation variances exceed the corresponding disturbance

variances in the evaluated systems. Weaker innovation autocorrelation should therefore not be interpreted as evidence of reduced variance.

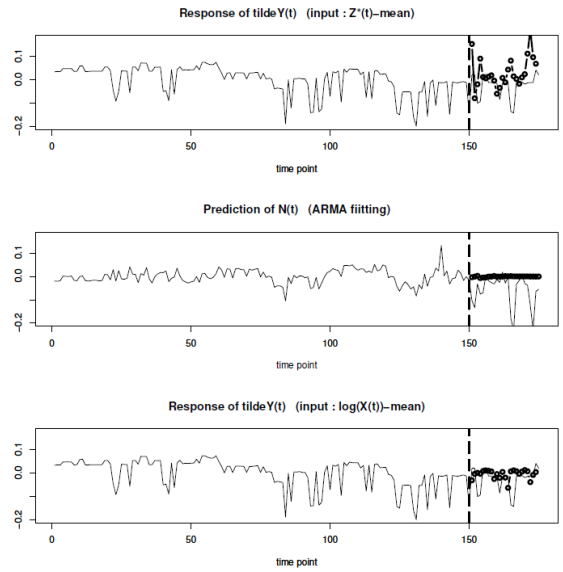


Figure 7: Model-based PF response and disturbance prediction (up to 25 steps ahead).

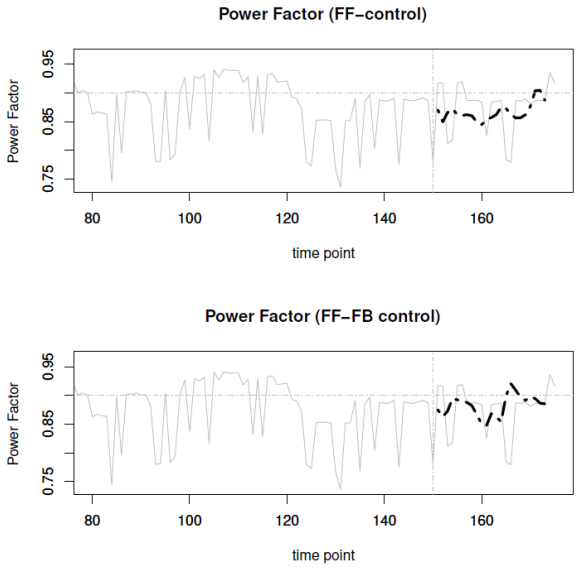


Figure 8: Simulated PF trajectories (up to 25 steps ahead; top: FF control; bottom: FF–FB control).

Figure 7 illustrates the model-based PF response and disturbance forecast over a 25-step horizon. Figure 8 compares simulated PF trajectories under feedforward (FF) and combined feedforward–feedback (FF–FB) control. Neither figure reports measured post-actuation results.

For the rolling-window robustness evaluation, e_k denotes the calculated one-step-ahead PF control deviation relative to the zero target reference. It is not an ordinary observed-minus-predicted forecasting residual. The downside frequency is $\rho_r = N(e_k < r)/N(e_k)$, for $r < 0$; smaller ρ_r means fewer large negative calculated control deviations.

Comparison of the two model strategies

The control-robustness measure ρ_r is compared at four negative thresholds. The six-system FF and FF–FB results appear in Appendix B (Tables B1 and B2), while the principal multivariable comparison is summarised here.

Control	Weighting	Mean error	ρ(−0.015)	ρ(−0.020)	ρ(−0.025)	ρ(−0.030)
FF	A	−0.0037	0.24	0.19	0.12	0.07
FF	B	−0.0036	0.22	0.14	0.10	0.05
FF–FB	A	−0.0052	0.30	0.23	0.16	0.12
FF–FB	B	−0.0049	0.29	0.20	0.18	0.09

For FF control, Method B shows lower downside frequencies than Method A at all four thresholds. At r = −0.020, the frequency falls from 0.19 (A) to 0.14 (B). A single-factor baseline nevertheless has the lowest frequency at r = −0.030 (0.04 versus 0.05 for B), so the finding is a consistent advantage for B over A, not superiority on every measure against every baseline.

Adding the ARMA-based feedback contribution did not improve the reported downside frequencies for either multivariable weighting method: FF–FB values exceed the corresponding FF values at all four thresholds. The result favours the simpler FF arrangement for the tested control-robustness criteria and operating record; it does not exclude benefits under other tuning or disturbance conditions.

The 100 evaluations shift through the measured operating sequence and therefore provide a repeated within-dataset comparison. Because consecutive estimation windows overlap, the frequencies are descriptive measures of the reported experiment rather than results of 100 independent trials.

Changing importance of monitored factors

Figure 9 shows how the Method B weighting changes across the 100 evaluation windows. Reactive power often receives a weight above the equal-share reference of 0.25, but its contribution falls during some periods as other observed factors become more influential.

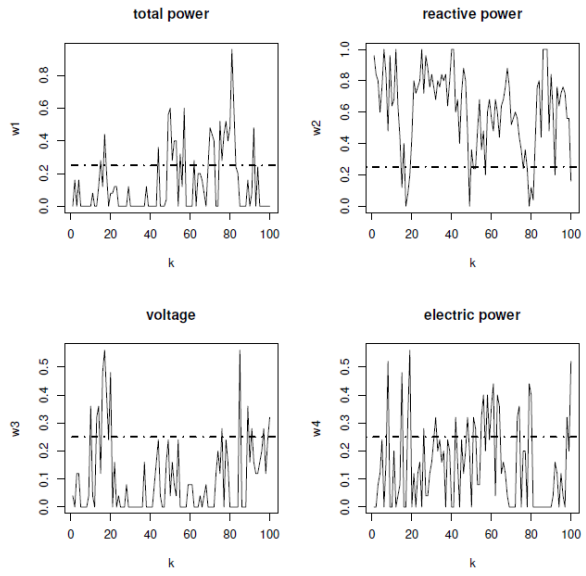


Figure 9: Estimated Method B factor weights by rolling window (upper left: total power; upper right: reactive power; lower left: voltage; lower right: electric power). Dashed line: equal weight of 0.25.

The changing weights indicate that the model adapts its predictive emphasis to the recorded operating conditions. They measure relative contributions within the selected statistical formulation, not a direct causal effect on PF.

Interpretation, limitations and practical significance

Box–Jenkins-guided numerical FF control with prediction-error weighting (Method B) produced fewer adverse calculated PF control deviations than fitting-error weighting (Method A) in the multivariable comparisons. FF–FB did not improve the selected downside frequencies. Method B also had the smallest reported disturbance variance among the six observation systems. These results come from numerical control experiments and simulation, not physically applied current adjustments.

The figures and rolling-window tables describe complementary aspects of the investigation: monitored electrical behaviour, simulated control responses and calculated robustness across changing data windows. The quantitative comparisons do not establish measured before-and-after effects of implementing a physical controller.

Further work may examine the stability of parameter estimation as cross-correlations change, the disturbance–innovation variance relationship, feedback tuning, sustained target tracking and replication on other machines or operating regimes. The results do not establish capacitor-bank replacement or quantified tariff savings. Related application of time-series control to industrial processes is documented in [20].

VI. CONCLUSION

This study applied Box–Jenkins transfer-function modelling to power factor management using measurements from an operating industrial robotic welding process. Dynamic relationships between PF and multiple monitored electrical factors were identified from measured time-series data, and calculated current-control strategies were evaluated through numerical experiments and simulation.

The multivariable method combines individual factor-specific transfer-function predictions in an overall PF-response model. In the reported rolling-window evaluation, prediction-error weighting (Method B) produced lower adverse negative-deviation frequencies than historical fitting-error weighting (Method A) across all four examined thresholds for feedforward control. The estimated factor weights also changed across operating windows, demonstrating an adaptive predictive emphasis.

Adding ARMA-based feedback did not improve the reported downside frequencies for either multivariable weighting strategy. This finding supports comparison of control strategies on their observed performance rather than assuming that additional complexity always improves outcomes.

The results demonstrate the application of Box–Jenkins-guided numerical current-control analysis and the comparative advantage of prediction-oriented weighting under the investigated conditions. Future research may examine physical implementation, actuator feasibility, welding-process constraints, sustained power factor target tracking, alternative feedback tuning, and integration with conventional reactive-power compensation systems. Further validation across different equipment and operating conditions would establish the broader applicability of the proposed approach. [21].

ACKNOWLEDGEMENTS

The authors would like to thank Mitsubishi Electric Malaysia Company, Takebishi Malaysia Company for the equipment support. The authors would like to express their gratitude to Ts. Dr. Lee Yoon Ket, Ir. Dr. Chiew Tsung Heng, Dr. Ong Jia Jan and Dr. Chang Kai Ming of Centre for Autonomous Systems and Robotics Research in Tunku Abdul Rahman University of Management and Technology, for providing the advisory and support to the research work.

DECLARATION OF COMPETING INTERESTS

The authors declare that they have no known competing financial interests or personal relationships that could have appeared to influence the work reported in this paper.

Data availability : The authors have shared data through the following link: https://github.com/ica40git/da_power_meter

REFERENCE

[1] Malaysia Ministry of Investment, Trade and Industry (MITI), Industry4WRD: National Policy on Industry 4.0, (https://www.miti.gov.my/index.php/pages/view/industry4WRD?mid=814),

(2018).

[2] K. D. Thoben, S. Wiesner, and T. Wuest, "Industrie 4.0" and Smart Manufacturing, A Review of Research Issues and Application Examples, Int. J. of Automation Technology, Vol.11, No.1, 4-16, (2017).

[3] A. Schumacher, S. Erol, and W. Sihn, A maturity model for assessing Industry 4.0 readiness and maturity of manufacturing enterprises, Procedia CIRP (Elsevier), Vol.52, 161-166, (2016).

[4] N. S. Bajaj, A. D. Patange, R. Jegadeeshwaran, S. S. Pardeshi, K. A. Kulkarni, and R. S. Ghatpande, Application of metaheuristic optimization based support vector machine for milling cutter health monitoring, Intelligent Systems with Applications, Vol.18, 200196, (2023).

[5] Standard and Industrial Research Institute of Malaysia (SIRIM), Guidelines for implementing Green 5S system, SIRIM 5, (2016).

[6] W. M. Z. W. Abdullah, W. N. R. A. Zainudin, and N. A. Ramli, A Proposed Model to Determine Public Acceptance on Willingness to Pay Maximum Demand (MD) Charge in Malaysia, Advanced Science Letters, Vol.24, No.11, 8917-8921, (2018).

[7] S. Bhattacharyya, A. Choudhury, and H. R. Jariwala, Case Study On Power Factor Improvement, International Journal of Engineering Science and Technology (IJEST), Vol.3, No.12, 8372-8378, (2011).

[8] M. N. Zaidi, A. Ali, Power Factor Improvement Using Automatic Power Factor Compensation (APFC) Device for Medical Industries in Malaysia, MATEC Web of Conferences 150, 01004, (2018).

[9] F. Y. Limpraptono, E. Nurcahyo1, M. I. Ashari, E. Yandri, and Y. Jani, Design of Power Monitoring and Electrical Control Systems to Support Energy Conservation, Proceedings of the Pakistan Academy of Sciences, A. Physical and Computational Sciences: 58(S): 1-7, (2021).

[10] O. I. Elgerd, Control of electric power systems, IEEE Control Systems Magazine, Vol.1, Issue.2, 4 - 16, (1981).

[11] J. D. Hamilton, State-space models, Handbook of Econometrics, Chapter 50, Vol. 4, 3039-3080, (1994).

[12] T. Higuchi, and G. Kitagawa, Knowledge Discovery and Self-Organizing State Space Model, IEICE Trans. Inf. & Syst., Vol. E00-A, No.1, (1999).

[13] G. Kitagawa, Use of a State Space Model in Time Series Analysis, Proceedings of the Institute of Statistical Mathematics, Vol. 67, No. 2, 181-192, (2019).

[14] P. C. Young, and D. E. Runkle, Recursive Estimation and Modelling of Nonstationary and Nonlinear Time-series, 3rd IFAC Proceeding Volumes, Vol. 23, Issue 1, 509-524, (1990).

[15] N. Kashiwagi, On Use of the Kalman Filter for Spatial Smoothing, Annals of the Institute of Statistical Mathematics, Vol.45, No.1, 21-34, (1993).

[16] G.E.P. Box, and G.M. Jenkins, Time Series Analysis, forecasting and control, Revised edition, Prentice Hall, New Jersey, (1976).

[17] S. Konishi, The Role of Information Criterion AIC in Statistical Science, Proceedings of the Institute of Statistical Mathematics, Vol.67, No.2, 193- 214, (2019).

[18] T. Hokimoto, K. Amagai, N. Kimura and M. Huzii, A predictor for sea surface movement by taking into account of possibility of nonstationarity, Istatistik, Vol.2, No.1, 41-55, (1999).

[19] M. S. Bartlett, Stochastic Processes, Cambridge University Press, Cambridge, (1955).

[20] S. Hagimura, T. Saitoh and Y. YAGIHARA, Application of time series analysis and modern control theory to the cement plant, Ann. Inst. Statist. Math., Vol.40, No.3, 419-438, (1988).

[21] T. S. Gunawan, M. H. Anuar, M. Kartiwi and Z. Janin, Design of power factor meter using internet of things for power factor improvement, remote monitoring and data logging, Indonesian Journal of Electrical Engineering and Computer Science, Vol.17, No.2, 700-709, (2020).

APPENDIX A. MATHEMATICAL FORMULATION AND DERIVATION

Appendix A specifies the transfer-function and ARMA framework. Equations (1)–(12) define the dynamic-response model, feedforward compensation, disturbance forecasting and feedback correction.

A.1 Definitions and combined response model

Let $\tilde{Y}_t = Y_t - \bar{Y}$ denote mean-centred PF, Z_t the mean-centred monitored voltage input, and X_t the current-related model input. Measured current and the controller-calculated current command have different operational meanings. The target deviation $Y_t - T$ is tracked separately. B is the backshift operator: $B^k U_t = U_{t-k}$.

(1) $\delta(B)\tilde{Y}_t = \theta(B)Z_{t-\beta} + nZ,_t$

Here $\delta(B) = 1 - \alpha_1 B - \ldots - \alpha_p B^p$ and $\theta(B) = 1 - \beta_1 B - \ldots - \beta q B^{\varphi}$. Under invertible $\delta(B)$:

(2) $\tilde{Y}_t = \delta^{-1}(B)\theta(B)Z_{t-\beta} + \tilde{n}Z,_t$

(3) $\tilde{Y}_t = L_1^{-1}(B)L_2(B)X_{t-}(f+1) + \tilde{n}X,_t$

The separate models do not automatically establish additive, independently identifiable effects. With that assumption explicitly stated, introduce $GZ(B) = \delta^{-1}(B)\theta(B)$ and $GX(B) = L_1^{-1}(B)L_2(B)$:

(4) $\tilde{Y}_t = GZ(B)Z_{t-\beta} + GX(B)X_{t-}(f+1) + N_t$

A.2 Feedforward cancellation

Set the two modelled input contributions to sum to zero. Assuming GX(B) admits a feasible inverse, shifting the time index by f+1 gives:

(5) $X_tFF = -GX^{-1}(B)GZ(B)\,Z_{t-(b-f-1)}$

Equation (5) is a theoretical feedforward current-control level for the numerical analysis, not a physically executed command. It requires an appropriately defined, causal and stable inverse $GX^{-1}(B)$; where $b - f - 1 < 0$, future voltage must be forecast. These conditions are not experimentally verified for an installed welding-machine controller. For changes in the setpoint, define:

(A1) $\Delta X_tFF = X_tFF - X_{t-1}FF = (1 - B)X_tFF$

An incremental controller would require a mechanism to reconstruct the intended level, including an initial condition. The timing condition $b - f - 1$ determines whether a historical/current voltage observation is available or a future voltage forecast is needed.

A.3 Residual forecasting and feedback

The ideal correction would cancel the disturbance at the time the current action takes effect:

(6) $X_tFB = -L_1(B)L_2^{-1}(B)\,N_{t+f+1}$

Because this future disturbance is unknown, assume an ARMA(r,m) process:

(7) $\varphi(B)N_t = \omega(B)a_t, \quad a_t \sim WN(0, \sigma a^2)$

For a causal and invertible representation, $N_t = \varphi^{-1}(B)\omega(B)a_t = [1 + \Sigma_{i=1}\infty\ \psi_iB^i]a_t$. Forecasting f+1 periods ahead from information available at t gives:

(8) $\hat{N}_t(f+1) = \psi f+1\ a_t + \psi f+2\ a_{t-1} + \ldots$

The disturbance forecast and the appropriately time-shifted prediction error are represented through the following filters:

(9) $\hat{N}_t(f+1) = L_3(B)a_t$

(10) $e_{t-f-1}(f+1) = L_4(B)a_t$

Provided that the required inverse exists, combine them to write $\hat{N}_t(f+1) = L_3(B)L_4^{-1}(B)e_{t-f-1}(f+1)$, leading to the stated feedback law:

(11) $X_tFB = -L_1(B)L_2^{-1}(B)L_3(B)L_4^{-1}(B)e_{t-f-1}(f+1)$

This equality is conditional on the chosen filter definitions, reliable innovation reconstruction and implementable inverse dynamics. It does not prove that an actual welding controller can directly deliver X_tFB.

A.4 Residual estimation under open- and closed-loop operation

The voltage-only baseline disturbance residual is estimated as follows:

(12) $rZ,j = \tilde{Y}_j - \hat{\delta}^{-1}(B)\hat{\theta}(B)Z_{j-\beta}$

This estimates N_j only when the modelled current-control contribution is zero or otherwise absent. During active current control, the combined-model residual is instead:

(A2) $\hat{N}_j = \tilde{Y}_j - \hat{G}Z(B)Z_{j-\beta} - \hat{G}X(B)X_{j-}(f+1)$

For a linear additive command model, the conceptual combination is:

(A3) $X_ttotal = X_tFF + X_tFB$

Equations (A2) and (A3) express the residual adjustment and combined current-control contributions under a linear additive model, subject to consistent variable definitions and identification assumptions.

APPENDIX B. MULTIVARIATE MODEL DETAILS AND EXTENDED EVALUATION

B.1. Multivariable formulations and model selection

In the multivariable formulation, factor-specific transfer-function outputs are combined into a composite observation series. Method A selects w to minimise historical squared errors L(w); Method B selects v to minimise one-step-ahead squared prediction errors S(v), with non-negative weights summing to one. The composite signal subsequently enters an overall transfer-function stage. Model orders are selected by AIC [17].

(B1) $Z^*_t = \Sigma_j\, w_j\, \delta_j^{-1}(B)\theta_j(B)B^{bj}Z_t^{(j)}, \quad \Sigma_j w_j = 1, \quad 0 \le w_j \le 1$

(B2) $Z^{**}_t = \Sigma_j\, v_j\, \hat{\delta}_j^{-1}(B)\hat{\theta}_j(B)\hat{Z}_{t-\beta j}^{(j)}, \quad \Sigma_j v_j = 1, \quad 0 \le v_j \le 1$

The multivariable response model includes a further observation-side transfer function: $\tilde{Y}_t = \delta_o^{-1}(B)\theta_o(B)Z^*_{t-\beta} + L_1^{-1}(B)L_2(B)X_{t-f-1} + N_t$ for Method A; an analogous $\delta_s^{-1}(B)\theta_s(B)Z^{**}_{t-\beta}$ term is used for Method B. The additional observation-side stage is retained in both model formulations.

Method A: $L(w) = \Sigma_t[\tilde{y}_t - \Sigma_j\, w_j\, \hat{\delta}_j^{-1}(B)\hat{\theta}_j(B)B^{bj}z_t^{(j)}]^2$; $\hat{w} = \arg\min L(w)$.

Method B: $S(v) = \Sigma_t[\tilde{y}_{t+1} - \Sigma_j\, v_j\, \hat{\delta}_j^{-1}(B)\hat{\theta}_j(B)\hat{z}_{t+1-\beta j}^{(j)}]^2$; $\hat{v} = \arg\min S(v)$.

For each j, the one-step-ahead input forecast $\hat{z}$ is constructed from a univariate time-series model where required. These objectives define the weighting procedures used in the numerical evaluation.

B.2. Rolling-window assessment and diagnostics

The target-relative logarithmic display uses $\tilde{Y}_t^* = \log(Y_t) - \log(T)$, with $T = 0.90$. In contrast, the general transfer-function derivation uses $\tilde{Y}_t = Y_t - \bar{Y}$. The logarithmic target-deviation display does not establish the estimation scale of every transfer-function coefficient.

The rolling-window procedure fits the response model using time points 1–150, forecasts the current variable one step ahead using ARMA, evaluates PF at time point 151, and advances the estimation window by five observations for each subsequent evaluation. One hundred evaluations are conducted across six observation systems: Methods A and B and the four individual electrical-factor models.

Downside frequency: $\rho_r = N(e_k < r) / N(e_k), \quad r < 0$

B.3. Nomenclature, symbols and abbreviations

Term / symbol	Meaning	Interpretation in this paper
PF / Y_t	Power factor	Measured power factor at time t; the principal electrical outcome.
T	PF target	Reference PF for assessment, fixed at 0.90 in this study.
P_t; Q_t	Active; reactive power	Measured electrical power quantities used to interpret PF.
Z_t	Monitored disturbance	Voltage in the single-input formulation; an observed input, not the commanded current.
X_t	Current-related variable	Measured current in the data; distinct from the controller-calculated current command.
X_tFF; X_tFB	Control components	Calculated feedforward and feedback current-control contributions.
ΔX_tFF	Incremental FF command	Change in feedforward current-control level between consecutive periods: $\Delta X_tFF = (1 - B)X_tFF$.
$\tilde{Y}_t$; $\bar{Y}$	Mean-centred PF; PF mean	$\tilde{Y}_t = Y_t - \bar{Y}$, where $\bar{Y}$ is the historical mean PF for the estimation period; distinct from target-relative deviation.
$\tilde{Y}_t^*$	Log target-relative PF deviation	$\tilde{Y}_t^* = \log(Y_t) - \log(T)$, with $T = 0.90$. Not additionally mean-centred; $\tilde{Y}_t^* = 0$ at the target.
B	Backshift operator	$BU_t = U_{t-1}$; represents time delays in the transfer function.
b; f+1	Response delays	Delay for monitored input and current-control response, respectively.
GZ(B); GX(B)	Transfer functions	Dynamic mappings from the observed input and control variable to PF response.
N_t	Unexplained disturbance	Remaining PF variation not explained by the modelled inputs.
a_t	ARMA innovation	New disturbance information after accounting for fitted temporal dependence.
ARMA	Autoregressive moving-average	Time-series model used to represent and forecast residual disturbance.
FF; FF–FB	Control strategies	Feedforward-only; combined feedforward–feedback control.
Method A; Method B	Multivariable weighting methods	Weights based on historical fitting error; weights based on one-step prediction error.

w_j; v_j; $\hat{v}_j$	Factor weighting coefficients	w_j: Method A weights; v_j: Method B weights; $\hat{v}_j$: estimated Method B weights in Figure 9. Each weight vector is non-negative and sums to one.
e_k	Calculated PF control deviation	One-step-ahead, target-relative calculated control outcome in rolling evaluation; not a conventional forecast residual.
ρ_r; r; N(·)	Downside frequency; threshold; count	$\rho_r = N(e_k < r)/N(e_k)$, $r < 0$; N(·) counts the evaluations satisfying the stated condition.
AIC	Akaike Information Criterion	Criterion used for transfer-function model-order selection.
$\hat{y}_t^{(j)}$; $\hat{y}_t$,obs	Factor prediction; combined prediction	Predicted PF contribution of factor j; weighted combined monitored-factor contribution in the weighted combination in Section IV
$X_t$total	Combined current-control command	Sum of FF and FB components under the additive model: $X_t\text{total} = X_tFF + X_tFB$.
φ(B); ω(B)	ARMA model polynomials	Autoregressive and moving-average polynomials respectively, in $\varphi(B)N_t = \omega(B)a_t$.
δ(B); θ(B)	Voltage-path model polynomials	Denominator (autoregressive) and numerator (input-response) polynomials for the voltage-to-PF transfer function in Appendix A.
$L_1(B)$; $L_2(B)$	Current-path model polynomials	Denominator and numerator polynomials in the current-to-PF transfer function, $GX(B) = L_1^{-1}(B)L_2(B)$.
$L_3(B)$; $L_4(B)$	Feedback forecast/error filters	Filters relating the disturbance forecast and shifted prediction error to the ARMA innovation in Appendix A.
j; k; t	Indices	j indexes monitored factors; k indexes rolling-window evaluations; t indexes time observations.
$nZ_{,t}$; $\tilde{n}Z_{,t}$; $\tilde{n}X_{,t}$	Single-input model disturbances	Disturbance terms in the separately fitted voltage- and current-response models in Appendix A; distinct from the combined residual N_t.
$rZ_{,j}$; $\hat{N}_j$	Estimated residuals	Voltage-only residual and combined-model estimated disturbance at observation j, respectively, in Appendix A.
$e_{t-f-1}(f+1)$; $\hat{N}_t(f+1)$	Forecast error; forecast disturbance	Lag-aligned prediction error and f+1-step-ahead conditional disturbance prediction in Appendix A; distinct from rolling-evaluation e_k.
α_i; β_i; ψ_i; σa^2	Model coefficients; variance	Coefficients of transfer-function and ARMA expansions, and ARMA innovation variance, in Appendix A.
Z^*_t; Z^{**}_t	Method A/B combined model terms	Weighted composite observation obtained from individually filtered factor inputs; followed by an overall observation-side transfer-function stage.
Var(N); Var(a)	Reported variances	Reported disturbance-residual and ARMA innovation variances; numerical results remain as reported in Appendix B.

B.4. Full results

Table B1. Feedforward-only results

System	Mean e	−0.015	−0.020	−0.025	−0.030
A	−0.0037	0.24	0.19	0.12	0.07
B	−0.0036	0.22	0.14	0.10	0.05
c	−0.0038	0.23	0.18	0.11	0.06
d	−0.0022	0.24	0.16	0.12	0.06
e	−0.0002	0.25	0.20	0.13	0.06
f	−0.0003	0.25	0.16	0.11	0.04

Table B2. Feedforward–feedback results

System	Mean e	−0.015	−0.020	−0.025	−0.030	Var(N)	Var(a)
A	−0.0052	0.30	0.23	0.16	0.12	0.0007	0.0011
B	−0.0049	0.29	0.20	0.18	0.09	0.0004	0.0016
c	−0.0051	0.27	0.19	0.16	0.10	0.0007	0.0008
d	−0.0023	0.25	0.18	0.12	0.07	0.0007	0.0025
e	0.0028	0.24	0.19	0.12	0.08	0.0007	0.0023
f	−0.0017	0.27	0.22	0.16	0.07	0.0007	0.0025

The reported Var (N) and Var (a) values are disturbance-residual and ARMA-innovation estimates, respectively. In all six systems, Var (a) exceeds Var (N); their direct statistical comparability has not been established. The numerical values are retained but are not used to infer variance reduction or improved physical control. The primary comparison instead relies on the reported rolling-window downside frequencies.